AUTONOMOUS TRACKING MODE WITH SPACE OBSERVATION RADAR: INITIAL ORBIT DETERMINATION AND TRACKING

M. Budoni[(1)], C. Carloni[(1)], D. Cerutti-Maori[(1)], and F. Piergentili[(2)]

[(1)] *Fraunhofer Institute for High Frequency Physics and Radar Techniques FHR, Fraunhoferstraße 20, 53343 Wachtberg, Germany, Email: {Matteo.Budoni, Claudio.Carloni}@fhr.fraunhofer.de*

[(2)] *University of Rome "La Sapienza", Department of Mechanical and Aerospace Engineering, Via Eudossiana 18, 00184 Rome, Italy*

ABSTRACT

This paper investigates the realization of an experimental autonomous tracking mode for the Tracking and Imaging Radar (TIRA), developed and operated by the Fraunhofer Institute for High Frequency Physics and Radar Techniques (Fraunhofer FHR). The final goal is to track autonomously any kind of space object crossing the radar field of view, without resorting to external information such as the two-line element sets.

Keywords: autonomous tracking; initial orbit determination; Kalman filtering.

1. INTRODUCTION

Currently, in order to acquire, detect and track a specific space object, the Tracking and Imaging Radar (TIRA) requires external information on its orbit. One source of such information is the U.S. Space Surveillance Network (SSN), which provides it in form of orbital elements (two-line element set, TLE) on [1]. Specifically, TIRA propagates the TLEs in order to predict the trajectory of a certain satellite and to rotate afterwards its antenna into the proper rendezvous position for the observation. The TLEs are regularly updated for circa 10000 catalogued space objects. However, in orbit there are many other objects smaller than about 10 cm (e.g. space debris) that are not yet catalogued. Therefore, no TLE data is available for them.

This is a problem of great importance since the number of this kind of objects is growing continuously. Among the causes of this constant growth, there is satellite fragmentation due to incidents (e.g. collisions and explosions), which can give birth to countless small particles that overcrowd the orbits. This is e.g. what happened in 1985 when an American anti-satellite missile mission destroyed the P78-1 Solwind solar observation satellite [2] or in 2007 when a Chinese rocket intentionally impacted a Chinese weather satellite [3].

It is of high interest to develop new tracking approaches for reconnaissance radar with tracking capabilities that shall grant, in the future, the autonomous tracking of space objects. The realization of such new operation modes is very important in order to allow the observations of any object crossing the antenna beam. These new tracking approaches can be used for instance to track multiple objects after their launch or the space debris created right after a fragmentation. This last aspect is necessary to avoid dangerous collisions with other satellites in the future following the debris creation.

This paper proposes a new autonomous tracking mode in Section 2, followed by the description of the experiment performed in order to validate it (Section 3 and Section 4). Lastly, the obtained results and the conclusions are shown in Section 5 and Section 6, respectively.

2. AUTONOMOUS TRACKING THROUGH AN OPEN LOOP MODE

The proposed scheme for the autonomous tracking mode with an open loop control consists basically of two phases: the initialization phase and the tracking phase [4]. During the initialization phase the antenna operates in beam park (BP) mode: i.e. it is fixed to a particular position monitoring a certain volume of the sky. When an object crosses the antenna beam, it is detected by the radar (detection step).

Then, the data obtained through this observation are processed by means of an initial orbit determination (IOD) algorithm in order to find an estimation of a future state vector for the detected object. Once this state vector is calculated and converted into an antenna position, the antenna rotates to this new foreseen rendezvous position (positioning step).

After this first antenna positioning, the tracking phase is initialized with the outputs of the IOD. This last phase is realized by processing data through a tracking filter, e.g. a Kalman filter (KF) [5]. The tracking consists in the alternating repetition of detection and positioning steps until the desired accuracy in the estimation of the state vector is achieved. This alternation is obtained through a succession of several BPs. The reason for selecting this

particular tracking scheme lies in the implementation of an open loop control strategy, which permits the radar to switch the observed object between two different BPs. As a consequence, this strategy manages to guarantee the multi-object tracking.
The whole designed autonomous tracking mode is shown as a flowchart in Figure 1. Starting from the top, the first step is the satellite detection. Then, the received radar raw data are transformed into observation vectors (range, range rate, azimuth, elevation). If the data are obtained during the first BP, they are processed by an IOD algorithm, otherwise they are processed by a tracking filter. In both cases, the output is a predicted state vector, which is used to compute the antenna position vector for the new antenna positioning step. Moreover, the predicted state vector is saved and used as the initial state vector of the subsequent tracking filter data processing.
For the initialization phase a new IOD algorithm adapted to the parameters of TIRA was developed and verified with TIRA. For the tracking phase two different kinds of filters were implemented: the Extended Kalman filter (EKF) and the Unscented Kalman filter (UKF). Also the performance of these tracking filters was evaluated with TIRA.

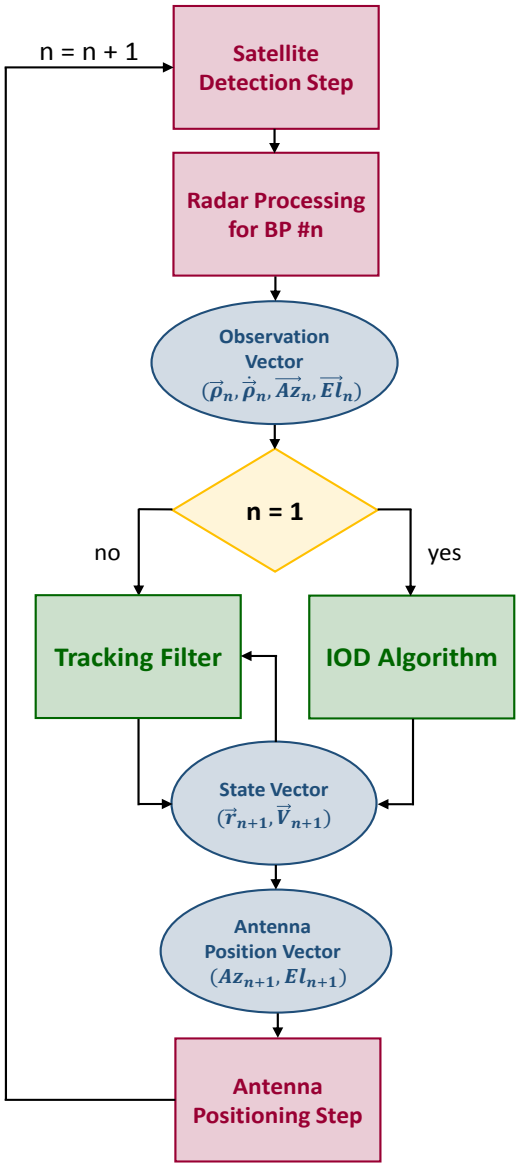

Figure 1. Autonomous tracking control scheme. The index n denotes the number of the actual beam park. On top, there is the detection of the satellite followed by the processing of the radar raw data, which gives in output a list of observation vectors. According to the value of n, these vectors are processed through an initial orbit determination algorithm or through a tracking filter. In both cases, the output is a predicted state vector for the satellite. This state is used to calculate the new antenna position and it is taken as the initial state of the subsequent filtering step. Finally, the antenna is re-positioned and the cycle is re-initialized updating the value of n.

3. MULTI BEAM PARK EXPERIMENT

In order to investigate the constraints related to the implementation of the proposed autonomous tracking mode for the TIRA system, a multi BP experiment was performed (Figure 2). It consists in the succession of several BPs realized at different elevation angles.
A very important facet of this kind of experiment is the investigation of the proper interval of time Δt_{BP} between two consecutive BPs. This Δt_{BP} (in black in Figure 2 between the first and the second BP) must be bound in a certain range included between a minimum value and a maximum value: $\Delta t_{\mathrm{min}} \leq \Delta t_{\mathrm{BP}} \leq \Delta t_{\mathrm{max}}$.
The lower limit, Δt_{min}, corresponds to the time required in order to accomplish all the technical processes. As shown in the zoom of Figure 2, it is given by the summation of three terms with different origins:

1. Δt_1, in orange, is the time associated to the radar data processing. Firstly, the radar raw data collected during the BP has to be processed in order to gain the observation vectors used as input by the IOD algorithm and by the KF. Secondly, the IOD algorithm and the KF have to calculate a state vector from the measurements and to propagate it in order to predict the future satellite position. As a consequence, Δt_1 has implications on the radar signal processing, on the IOD algorithm implementation and selection and on the tracking algorithm choice. The evaluation of this interval of time is one of the goals of the investigation performed in the paper.

2. Δt_2, in violet, is the time needed to rotate the antenna to the new predicted rendezvous position. TIRA, with its azimuth velocity of $24°$/s, is able to fulfil a total rotation in azimuth in 15 s. Within the same time, with its elevation velocity of $6°$/s, TIRA can move by $90°$ in elevation. Therefore, since two consecutive beam parks are generally spaced closely enough, this Δt_2 was assumed to be around 10 s in the worst case.

3. Δt_3, in light blue, is a safety margin, assumed to be around 5 s. It is the interval of time that occurs after the antenna is re-positioned and before the satellite crosses the beam. This interval is necessary since it has to be ensured that the radar is already transmitting when the satellite passes. Moreover, with this safety margin, it is possible to fix potential inaccuracies on the orbit parameters without compromising the success of the experiment.

The upper limit is $\Delta t_{\max}$, which is no longer related to any technical process, but to the accuracy achieved in the state vector estimation. In fact, both with the IOD algorithm and with the KF, there is always a certain error in the estimation of the state vector, especially in the velocity components. This error involves an inaccurate prediction of the future satellite position. Thus, if the propagation time is too long, the foreseen state is too inaccurate and no valid rendezvous position can be provided to the radar in order to detect again the satellite. As a consequence, the evaluation of this $\Delta t_{\max}$ is an important goal of the paper investigation.
Another crucial parameter, introduced in Figure 3, is the angle α (in violet) between the direction of the antenna and the satellite predicted line of sight (LOS). Also α

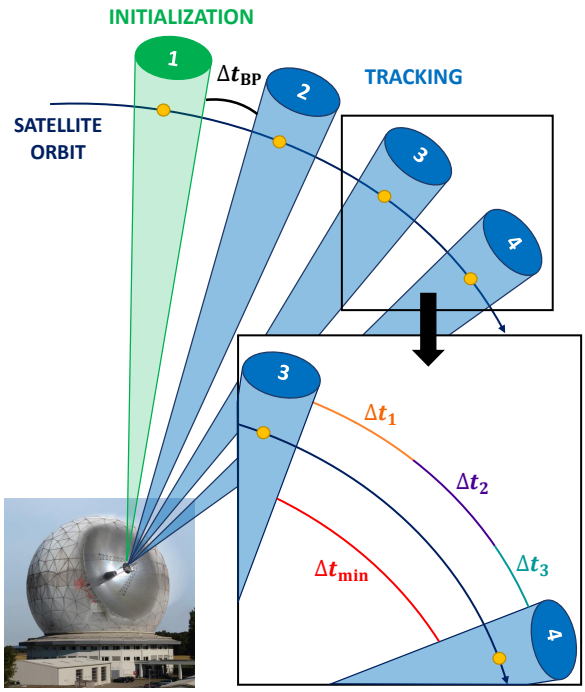

Figure 2. Multi beam park experiment and minimum time constraint. The main figure shows the design of the experiment adapted to the proposed autonomous tracking mode. Four beam parks (BP) are depicted: the first (in green) is linked to the initialization phase, the others (in blue) to the tracking phase. Δt_{BP} is the time between two different BPs. The zoomed square shows the minimum time constraint Δt_{min} along with its three components: Δt_1, related to the data processing, Δt_2, related to the antenna re-positioning, and Δt_3, a safety margin.

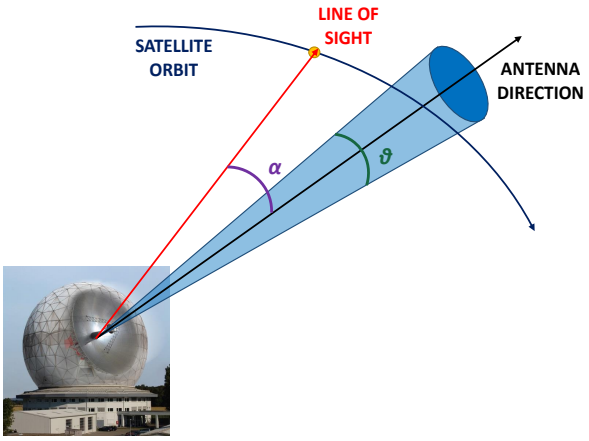

Figure 3. Geometry of the angles θ and α. θ is the 3 dB beam width of the antenna. α is the angle between the satellite line of sight and the direction of the antenna.

depends on the state vector estimation accuracy, as well as $\Delta t_{\max}$. After each positioning step, it has to be ensured that the object crosses again the antenna beam. This is achieved by evaluating this angle α. In fact, if α is smaller than a certain constraint, it is safe to assume that the foreseen satellite position would effectively be within the antenna beam. Since TIRA's antenna 3 dB beam width θ (in green) is about $0.5°$, the limit on α was chosen as $0.25°$, i.e. the half of the 3 dB beam width.
The same angle of $0.25°$ was taken also as the error limit on azimuth and elevation. Hence, in order to conclude that the radar is able to re-detect the satellite, it is important to compute its predicted position with an accuracy of $0.25°$ in azimuth and elevation.

4. PERFORMED EXPERIMENT

During the performed experiment, a pass of Envisat [6] was observed on February 2, 2018, at 7:40 UTC. The TLE used by the radar system to detect the satellite is shown in Table 1. A large object, such as Envisat, was selected for the experiment, in order to evaluate the constraints of the mode in the "best case scenario". In fact, this kind of satellites have a large radar cross section (RCS), which leads to higher signal to noise ratios (SNR) compared to the objects with a small RCS. Consequently, a high accuracy on the observation vectors can be ensured depending on the pass geometry.
The experiment is a multi BP investigation, as described in Section 3. During the whole satellite pass (time duration of about 14 min), 33 BPs were realized with a time spacing Δt_{BP} around 25 s. In order to choose this value for Δt_{BP} during the experiment design, it was assumed that 10 s was a good estimation for Δt_1.
Since the introduced autonomous tracking mode is not yet operational, Envisat was observed simply using the TLE propagation. Hence, all the proper antenna positions were not calculated in real time, because they were already known a priori. Nonetheless, this experiment was

Table 1. TLE used for the performed experiment.

```
Envisat
1 27386U 02009a   18033.15936933  .00000008  00000+0  16304-4 0  9996
2 27386  98.2025  73.4603 0001366  82.8178 277.3177 14.37914520834125
```

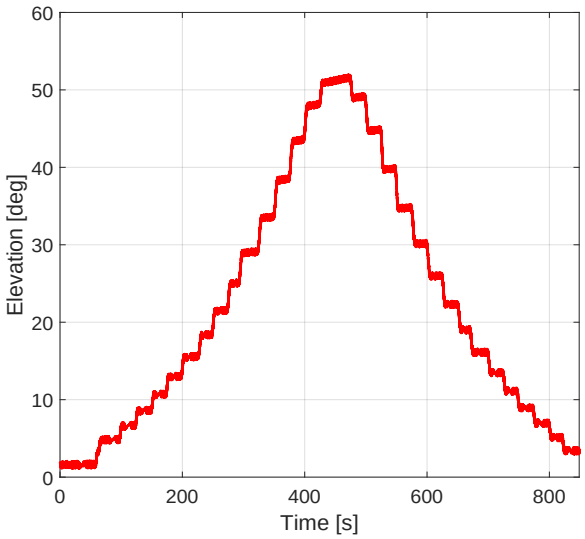

Figure 4. Elevation of Envisat. Envisat elevation is measured by TIRA with respect to the experiment relative time, which starts with the first observation. Each "step" represents a beam park.

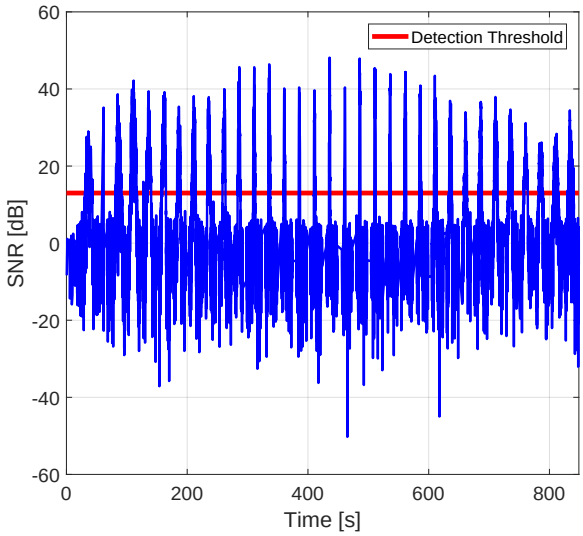

Figure 5. Signal to noise ratio (SNR) for Envisat. Envisat SNR is depicted with respect to the experiment relative time, which starts with the first observation. Each "peak" represents a beam park. The horizontal red line at 13 dB is the detection threshold.

realized to verify the performance of the various proposed algorithms, by comparing a posteriori the achieved results with the real observation measurements. This comparison entails an offline processing and not a real time one.

Figure 4 shows the elevation angle in degrees with respect to the relative time of the observation. This variable begins from low values, reaches a maximum around $52°$ and then decreases again to low values until the satellite disappears under the horizon.

An important parameter that is obtained from the radar raw data is the SNR, which indicates how accurate a certain measurement is. Figure 5 depicts the SNR during the whole experiment. From this figure, it is possible to notice a threshold at 13 dB that indicates the limit set for the satellite detection (the horizontal red line). Under this threshold it is assumed that the signal received by the radar contains only noise. On the other hand, over this limit, it is considered that the received signal contains also the object signal in addition to the noise.

There is a relation between the SNR and the elevation angle. When the elevation is low, the SNR is low while when the elevation is high, also the SNR is high. In contrast with this SNR behaviour, the radar data acquisition phase is longer for low elevation angles (longer beam crossing duration), while it is shorter for high elevation angles (shorter beam crossing duration).

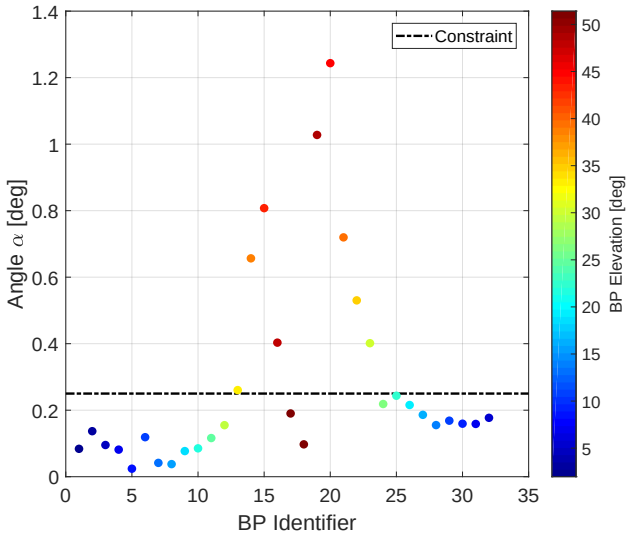

Figure 6. Behaviour of the angle α. The results for the angle α achieved using the proposed initial orbit determination algorithm are shown with respect to the beam park analyzed and to its elevation. The black horizontal dashed line is the $0.25°$ constraint.

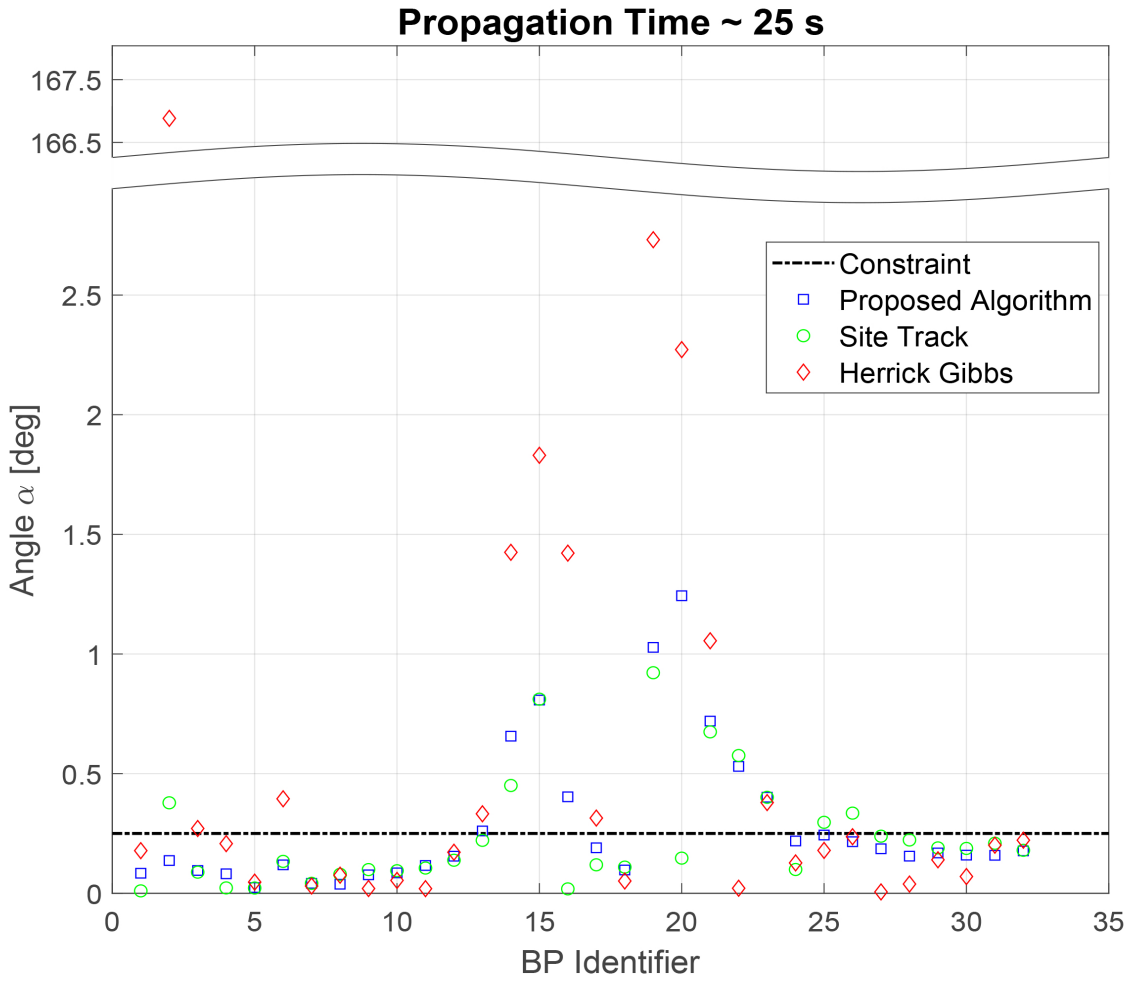

Figure 7. Comparison of the three initial orbit determination methods: the proposed one, the site-track and the Herrick-Gibbs. The results achieved for the angle α with the three different algorithms are compared. The black horizontal dashed line is the $0.25°$ constraint. In this case the propagation time is $\Delta t_{BP} \sim 25$ s.

5. RESULTS

The results achieved for the conducted experiment are discussed in two different subsections. The first one concerns the initialization phase and, consequently, the IOD algorithms performance. The second one belongs instead to the tracking phase and to the filtering process. Further in-depth studies and results regarding the two phases can be found respectively in [7] and [8].

5.1. Initial Orbit Determination

When an unknown object crosses the antenna beam during a BP, the radar system produces several measurements in a short time interval, related consequentially to a limited arc of the orbit. With such a short interval, an IOD is necessary to estimate the object orbit (in terms of orbital parameters or of state vectors). Currently, there are several algorithms in the literature used to solve the IOD problem. A list of the main algorithms together with their descriptions can be found in Chapter 7 of [9].
In this paper there is a comparison between the results achieved with three different algorithms: the new one developed [7], the site-track (ST) [9] and the Herrick-Gibbs (HG) [10]. The ST is a method which requires as input the following sensor data: range, range rate, azimuth, azimuth rate, elevation and elevation rate. This method is able to give a complete state vector (position and velocity) for the satellite in correspondence with each data set. The HG is one of the so called "three points methods" because it requires in input three different position vectors. It gives as output the velocity vector at the central point, providing thus only one complete state vector. The ST is very precise but not widely used because generally the sensors can not provide all the necessary data. On the contrary, the HG is widely used because it is relatively easy to find three position vectors.
TIRA can supply for each pulse the target range, range rate, azimuth and elevation. Thus, to apply the ST method, the estimation of two variables is necessary. Moreover, through a BP, TIRA gives a lot of data sets,

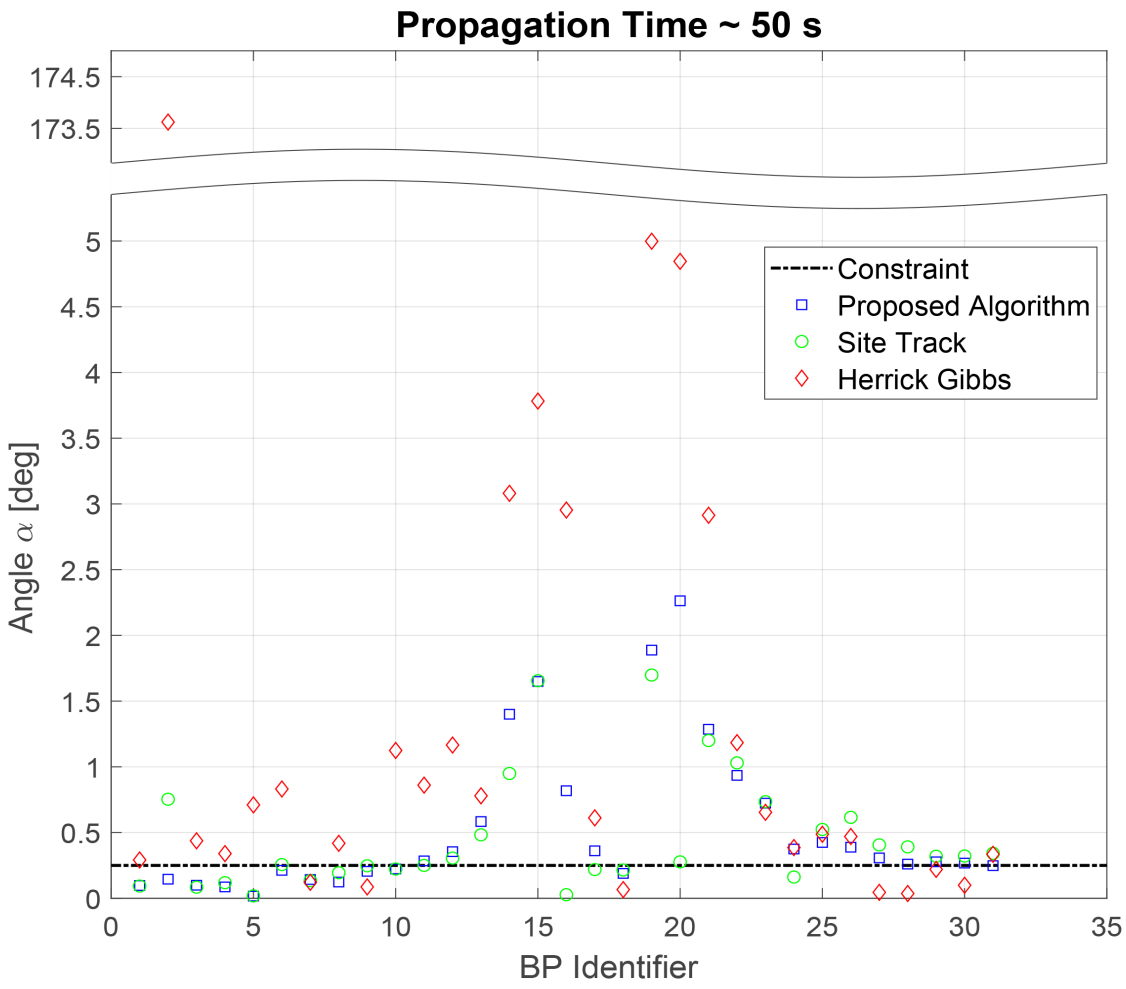

Figure 8. Comparison of the three initial orbit determination methods: the proposed one, the site-track and the Herrick-Gibbs. The results achieved for the angle α with the three different algorithms are compared. The black horizontal dashed line is the $0.25°$ constraint. In this case the propagation time is $\Delta t_{BP} \sim 50\,s$.

which involve the knowledge of much more than just three position vectors. For these two reasons a new IOD method was implemented: this method uses in input exactly the four kinds of data supplied by TIRA and accepts any number of data sets.

The scheme of the proposed autonomous tracking provides that just the first observed BP is processed with an IOD algorithm. Therefore, a crucial step is to understand with which BP elevation the best results are obtained. With regards to this topic, as discussed in Section 4, there are two main aspects that must be taken into account: the measurements SNR and the observation time duration. In order to find in correspondence with which BP elevation the algorithms perform better, all the observed BPs were analyzed individually, processing the measurements with the three IOD methods.

The variable studied in this investigation is the angle α, already shown in Figure 3. Since there are several consecutive BPs and in each of them the direction of the antenna is well known, it is effectively possible to compare the predicted antenna position with the real one by evaluating α.

An example is discussed here in order to clarify this aspect. The data obtained through the first BP are processed with one of the IOD methods: the algorithm gives as output the predicted position of the satellite in a future instant of time included in the second observed BP. From this position, it is possible to calculate the satellite LOS vector. This direction, according to the algorithm, is the one in which the antenna shall be positioned in order to re-detect the satellite in that future instance. However, in this experiment the new direction of the antenna is given because, using the TLE, the satellite was successfully re-detected and observed during the second BP. Therefore, comparing the predicted satellite LOS vector with the real antenna direction, it is possible to assess whether or not the satellite crosses again the antenna beam in the subsequent BP with the gained estimation. This is accomplished by checking if the angle α respects the imposed constraint of $0.25°$. If this occurs, the satellite detection is possible.

With the set SNR threshold of 13 dB, all the BPs have a big range of variation on the SNR, which has a global maximum of 48 dB. Since the proposed IOD method uses

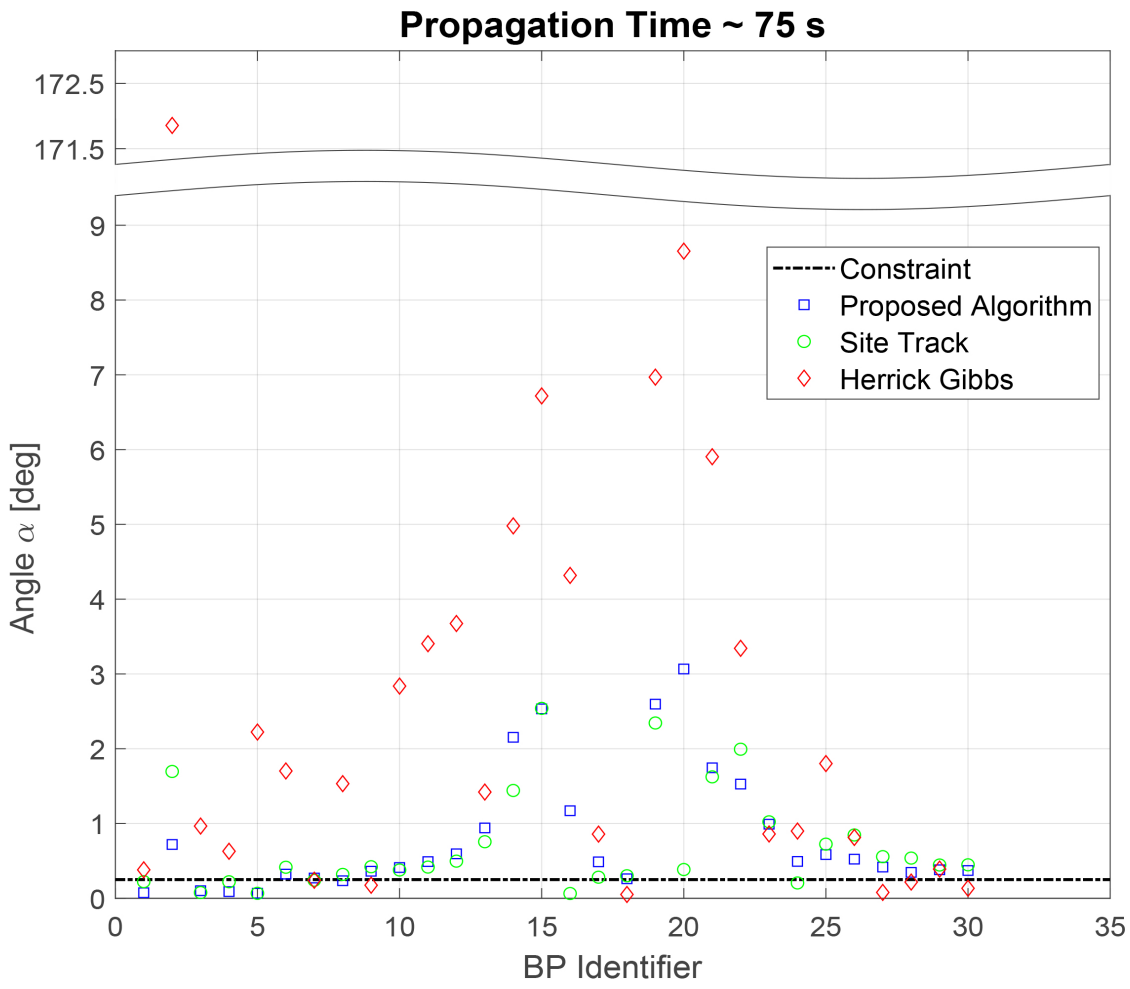

Figure 9. Comparison of the three initial orbit determination methods: the proposed one, the site-track and the Herrick-Gibbs. The results achieved for the angle α with the three different algorithms are compared. The black horizontal dashed line is the $0.25°$ constraint. In this case the propagation time is $\Delta t_{BP} \sim 75$ s.

all the provided data sets, there is the necessity of weighing the measurements in order to give more importance to the ones with an higher SNR, which are more accurate. The used weights were taken equal to the SNR values.

The results of the analysis for the new developed algorithm are shown in Figure 6, where the angle α is depicted with respect to the BP analyzed and to its elevation. The colorbar indicates for every BP the corresponding elevation. The angle constraint of $0.25°$ discussed in Section 4 is included in the figure as a black horizontal dashed line. It is possible to see from the graphic that only the first 32 BPs were processed. Indeed, since there is no 34th BP, the results achieved for the 33rd one could not be compared with any direction of the antenna. Therefore, no result is given for it.

Figure 6 shows that the obtained angle α is almost always included in the constraint, apart from nine cases. Moreover, it points out that the results are more accurate in correspondence with the low-elevation BPs. In fact, all the failures are registered when the elevation is high.

The same analysis was performed for the other two IOD algorithms: the ST and the HG. In Figure 7 the results are compared for all the three different methods. Here there is no longer the colorbar, but the elevation follows the same trend as in Figure 6 (namely low, high and low again).

For the second BP, the angle α obtained with the HG turns out to be almost $167°$. This is due to the fact that the second BP has a time duration that is very short (shorter than 1.5 s) because the satellite did not cross the beam close to its center. With such a short interval, the HG method fails in finding a good estimation for the satellite velocity vector. Thus, the predicted position for the satellite is very far from the real one.

Figure 7 shows that the ST fails nine times while the HG fails twelve times. All the three algorithms highlight that the best situation for the observation of a space object is to have a BP at low elevations. In fact, with low elevations, in this experiment it is almost always possible to re-detect the satellite. The failures correspond generally to the BPs realized at higher elevations.

In order to investigate the upper time constraint $\Delta t_{\max}$, discussed in Section 3, the same analysis was realized using a Δt_{BP} around 50 s and around 75 s, i.e. comparing

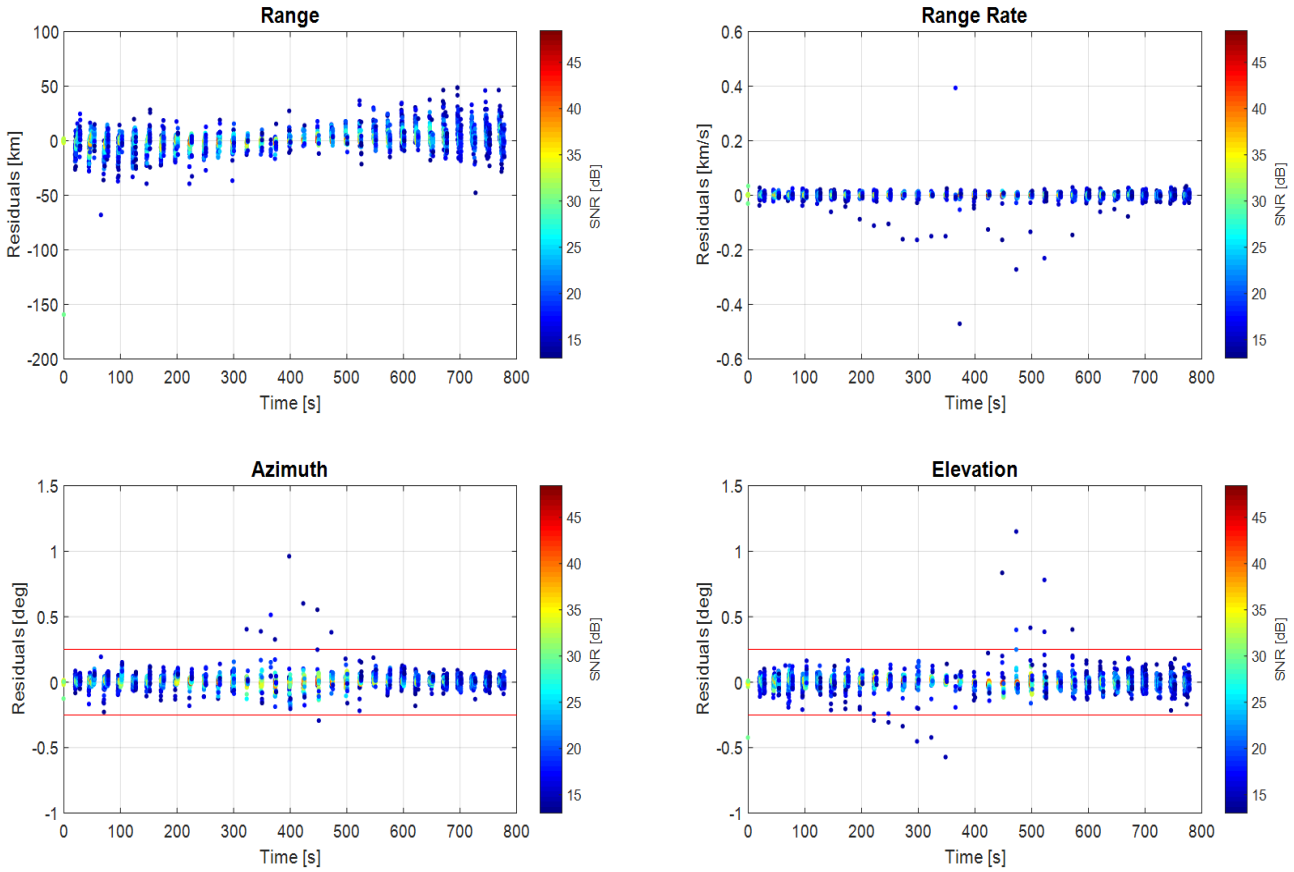

Figure 10. Relative observation residuals for the Extended Kalman filter (EKF) on range (top left), range rate (top right), azimuth (bottom left) and elevation (bottom right). The relative residuals are computed as the difference between the predicted state vectors of the EKF, transformed into observation vectors, and the measurements coming from TIRA (with a signal to noise ratio threshold of 13 dB).

the results of each BP with the BP performed respectively two or three later. Also in these two cases the comparison between the three different IOD methods has been realized. The achieved results are shown in Figure 8 and in Figure 9. Here, the total number of BP investigated is 31 and 30, respectively. The elevation trend is always the same as in Figure 6. Also for these last two investigations, the angle α related to the second BP obtained with the HG is in the order of 170°.

Figure 8 shows that with a Δt_{BP} of 50 s the proposed algorithm fails 20 times, the ST 19 times and the HG 17 times, while Figure 9 shows that with a Δt_{BP} of 75 s the proposed algorithm fails 25 times, the ST 23 times and the HG 24 times. Both the figures point out once more that the best results are obtained at low-elevation BPs. In these last two analysis there are more failures respect to the first one because the prediction accuracy is smaller. This happens since, as explained in Section 3, the error on the estimation of the orbit parameters has a bigger impact on the position prediction when it is propagated for longer times. Therefore less accurate predicted state vectors are achieved.

5.2. Kalman Filtering

Two different kinds of KFs were investigated: the Extended KF (EKF) and the Unscented KF (UKF). The EKF is one of the most used estimation algorithm for nonlinear systems (Chapter 10 of [9]). However, it is difficult to implement and to tune and above all, it is reliable especially for systems that are almost linear. The UKF is introduced to face these problems [11]. In fact, thanks to the unscented transformation, a new approximate method for propagating means and covariances through nonlinear transformations is used.

The KF is initialized with the outcomes of the IOD. The state vector given by the IOD is propagated until the subsequent BP acquisition phase. The acquired radar data are processed by means of a KF. The low elevations recorded at the beginning of the experiment allow the IOD and the KF to process more measurements and to estimate better the state vector.

Figure 10 shows the relative residuals (R_{rel}), which are computed as the difference between the observation vectors calculated from the predicted state vectors of the EKF (Y_{KFprop}) and the measurements coming from TIRA (Y_{meas}): $R_{\mathrm{rel}} = Y_{\mathrm{KFprop}} - Y_{\mathrm{meas}}$.

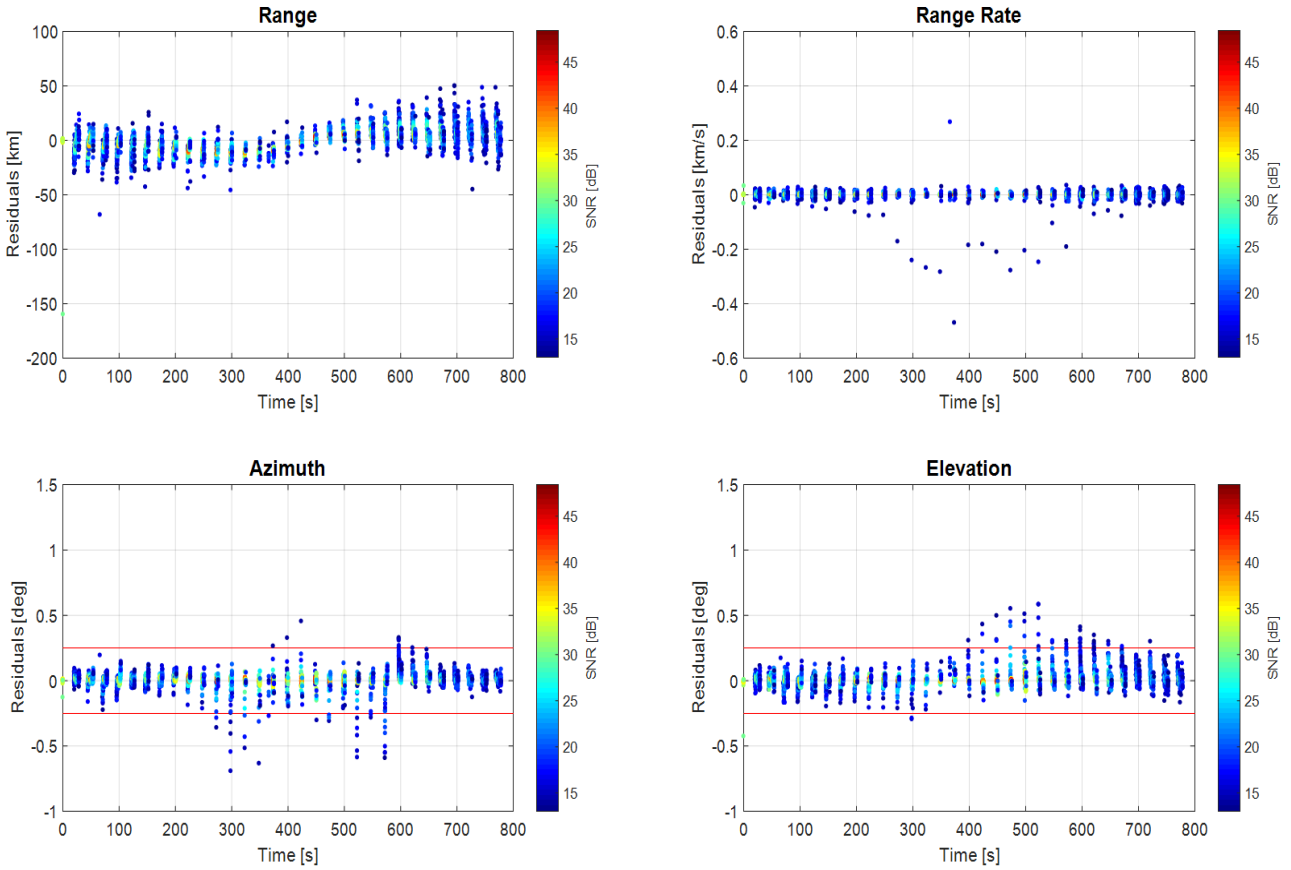

Figure 11. Relative observation residuals for the Unscented Kalman filter (UKF) on range (top left), range rate (top right), azimuth (bottom left) and elevation (bottom right). The relative residuals are computed as the difference between the predicted state vectors of the UKF, transformed into observation vectors, and the measurements coming from TIRA (with a signal to noise ratio threshold of 13 dB).

Since the true trajectory of the object is unknown, the only possible comparison a posteriori is with the radar measurements. These have different accuracies, which are reflected in the figure by the colorbar of the SNR. The starting point of the colorbar is 13 dB, i.e. the selected SNR threshold.

The residuals on azimuth and elevation are most of the time within the boundary condition of $\pm$ 0.25°. Even when the residuals are off the limits, it is not sure that the target is lost. In fact, the residuals are calculated with respect to the measured observation vectors which have already a certain intrinsic error, embodied by their accuracy (σ). The largest residuals are achieved in correspondence with the blue SNR, i.e. where the σ on the measurements is higher. Therefore no final conclusion can be drawn from this graph. Nonetheless, looking at the residuals on the angles, it is possible to notice how their dispersion increases in the middle of the pass, when the elevation of the satellite is higher. This happens because around the closest approach the time spent by the satellite inside the beam is shorter. Consequently, the margin of error to redetect the object is reduced.

Concerning the UKF, the results shown in Figure 11 are computed in the same way as for the EKF. The relative residuals have almost the same trend and the same considerations can be made once more. The residuals increase in the middle of the pass, even if in this case they are slightly lower.

Although the EKF and the UKF give very similar results in terms of relative residuals, they have a different behaviour concerning the covariance matrix information. Figure 12 and Figure 13 show the covariance ellipsoids referred to the third beam park for the EKF and the UKF, respectively. The covariance ellipsoid dimensions reflect the reliability of the state vector coming from the filtering process. In each figure, two different ellipsoids are presented. The larger one is the covariance ellipsoid associated to the instant of time just before the acquisition phase, i.e. at the end of the propagation phase. Instead, the smaller one is the covariance ellipsoid associated to the instant of time right after the acquisition phase. The covariance ellipsoids are both rotated in the body reference frame: two directions are in the orbit plane (radial and along-track), while the third direction is normal to the orbit plane (cross-track). Looking at both the figures, there is a large difference in the covariance ellipsoid dimensions. Specifically, the UKF ellipsoid after the propagation time is smaller than the correspondent EKF ellipsoid. Conversely, the UKF covariance ellipsoid dimensions after the acquisition phase have the same size order

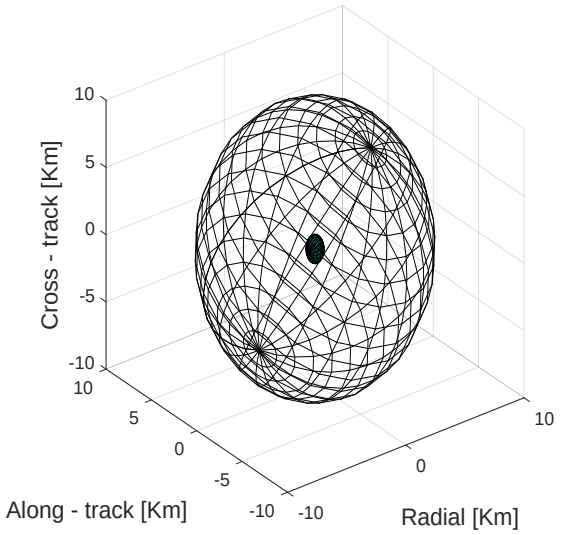

Figure 12. Covariance ellipsoids calculated from the covariance matrix of the Extended Kalman filter. They refer to the third beam park. They are rotated in the body reference frame (radial, along-track, cross-track). The larger ellipsoid is computed in the instant of time just before the acquisition phase, while the smaller ellipsoid in the instant of time right after the acquisition phase.

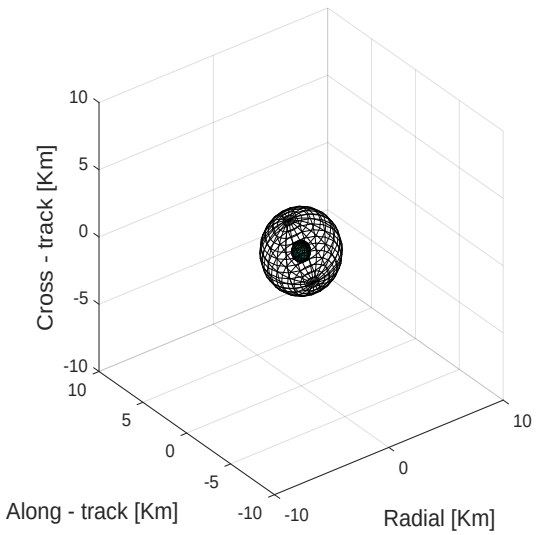

Figure 13. Covariance ellipsoids calculated from the covariance matrix of the Unscented Kalman filter. They refer to the third beam park. They are rotated in the body reference frame (radial, along-track, cross-track). The larger ellipsoid is computed in the instant of time just before the acquisition phase, while the smaller ellipsoid in the instant of time right after the acquisition phase.

of the EKF ones. This means that the main difference between the two KFs is in the propagation of the covariance matrix. The covariance matrix in the EKF is just propagated through a transition matrix, which represents only a first order linearization of the dynamic model. On the contrary, the UKF works by constructing a set of sigma points, accurately chosen, which represents statistically the true mean and covariance information. Each sigma point is propagated through the non-linearity using directly the dynamic model, without any linearization. Afterwards, a recombination of the propagated sigma points is performed in order to obtain the new state vector and the new covariance matrix. This latter is more accurate than the EKF one because it takes into account also terms of higher orders [12].
From the computational cost point of view, the EKF is more efficient since in the EKF just one state vector is propagated. In fact, the extra effort of the UKF is related to the number of sigma points, which have to be propagated one by one and mixed together in order to find the new state vector.

6. CONCLUSIONS

This paper presented an autonomous tracking mode for the TIRA system and demonstrated the implemented algorithms with real data. They were tested only with one large object (i.e. Envisat), therefore no general judgement can be made from this investigation.
The analysis performed illustrates that the proposed methods are more accurate for the BPs at low elevations. For this reason, it is reasonable to assume that the best configuration to initialize the autonomous tracking mode is with the antenna pointing towards low elevations.
Two time constraints were investigated in this paper: Δt_1 and $\Delta t_{\max}$, both discussed in Section 3. Δt_1 consists of two different contributions. The first one is linked to the radar raw data processing and it can not be evaluated through this experiment because the analysis was realized a posteriori. The second one is related to the computational cost of the used algorithms in each single BP. This study has found that this term is in the size order of 5 s (no code optimization was performed). Section 5.1 shows the results of the IOD for three different values of Δt_{BP} in order to evaluate $\Delta t_{\max}$. Increasing the value of Δt_{BP}, the results become less accurate because the error on the estimation is propagated for longer time. This investigation reveals that even with a propagation time of 75 s, for some of the low-elevation BPs it is possible to re-detect the satellite.
The comparison between the different IOD algorithms shows that the performance of the three methods is almost equivalent, with the HG having the highest variability. Nonetheless, it has to be noted that in terms of computational cost, the proposed algorithm is outperformed by the others because it processes much more data sets for finding one single state vector. However, even with this algorithm the computational time is still quite short. Specifically, it depends on the beam crossing duration. Longer beam crossing durations correspond to more measurements to process and consequently the computational time increases. This time can be reduced in the future by some optimization processes.
Concerning the tracking part, the two different KFs are both able to track the object during almost the whole pass,

with some uncertainties when the elevation is higher. In fact, it is not possible to assess a potential target loss just from a relative comparison of the residuals. However, an accurate orbit determination depends on a lot of parameters (e.g. RCS, observation geometry, SNR, elevation). Therefore a choice between the two different KFs is needed. From a reliability point of view, the UKF is more efficient in terms of the covariance matrix propagation. Instead, concerning the computational cost, the UKF requires more time. This is due to the number of sigma points, which have to be propagated one by one and to be mixed together in order to have the new state vector, while in the EKF just one state vector is propagated. A trade-off between the accuracy of the covariance information and the computational cost is needed in order to select the best KF. In the literature, it is possible to find other kinds of UKF like the Scaled UKF [13] or the Reduced Sigma Point filter [14], that have been developed in order to reduce the UKF computational time, without undermining its precision.
As described in Section 4, this experiment was performed as an offline processing. In the near future, other objects (smaller than Envisat and with different orbits) will be observed with the same kind of experiment in order to verify the findings obtained in this paper. Lastly, the final step will be the realization of a completely autonomous real time procedure, which requires the implementation of the investigated algorithms in the TIRA system.

REFERENCES

1. T. S. Kelso, *Celestrak*. Retrieved from https://www.celestrak.com/
2. J. M. Guilfoil (26.7.2012), *ASM-135 ASAT*. Retrieved from http://theaircache.com/2012/07/26/asm-135-asat/
3. L. David (2.2.2007), *China's Anti-Satellite Test: Worrisome Debris Cloud Circles Earth*. Retrieved from https://www.space.com/3415-china-anti-satellite-test-worrisome-debris-cloud-circles-earth.html
4. G. Ruiz, T. Patzelt, L. Leushacke, O. Loffeld, *Autonomous Tracking of Space Objects with the FGAN Tracking and Imaging Radar*. Fraunhofer FHR (2006)
5. R. E. Kalman, *A New Approach to Linear Filtering and Prediction Problems*. Transactions of the ASME-Journal of Basic Engineering, 82 (Series D): 35-45. Copyright by ASME (1960)
6. H. J. Kramer, *EnviSat (Environmental Satellite)*. Retrieved from https://eoportal.org/web/eoportal/satellite-missions/e/envisat
7. M. Budoni, *Development and Experimental Testing of an Initial Orbit Determination Algorithm based on Radar and Optical Data*. Master Thesis Project, University of Rome "La Sapienza" - Fraunhofer FHR (2018)
8. C. Carloni, *Tracking filters for orbit determination from radar and optical measurements*. Master Thesis Project, University of Rome "La Sapienza" - Fraunhofer FHR (2018)
9. D. A. Vallado, *Fundamentals of Astrodynamics and Apllications*. Fourth Edition, Space Technology Library (2013)
10. S. Herrick, *Astrodynamics: Orbit Determination, Space Navigation, Celestial Mechanics*. Vol. I, Van Nostrand Reinhold Co. (1971)
11. S. J. Julier, J. K. Uhlmann, *New extension of the Kalman filter to nonlinear systems*. Proceedings SPIE 3068, Signal Processing, Sensor Fusion, and Target Recognition VI, (28 July 1997); doi: 10.1117/12.280797
12. S. J. Julier, J. K. Uhlmann, *Unscented Filtering and Nonlinear Estimation*. Proceedings of the IEEE (Volume: 92, Issue: 3, Mar 2004), 8 November 2004
13. S. J. Julier, IDAK Industries, *The Scaled Unscented Transformation*. Proceedings of the 2002 American Control Conference (IEEE Cat. No.CH37301), Anchorage, AK, USA, 8-10 May 2002
14. S. J. Julier, J. K. Uhlmann, *Reduced Sigma Point Filters for the Propagation of Means and Covariances Through Nonlinear Transformations*. Proceedings of the 2002 American Control Conference (IEEE Cat. No.CH37301), Anchorage, AK, USA, 8-10 May 2002